Weakly nonlinear of Marangoni instabilities in an evaporating liquid layer

M. Dondlinger*, J.Margerit and P.C. Dauby
Université de Liège, Institut de Physique B5a,
Allée du 6 Août 17, B-4000 Liège, Belgium

preprint for Journal of Colloid and Interface Science 283 (2005) 522-532

Abstract

We propose a theoretical study of Marangoni driven convection in an evaporating liquid layer surmounted by an inert gas-vapor mixture. After reduction of the full two layer problem to a one-sided model we use a Galerkin-Eckhaus method leading to a finite set of amplitude equations for the weakly nonlinear analysis of the problem. We analyse the stability of the roll, square and hexagonal patterns emerging above the linear stability threshold for a water-air and for an ethanol-air system.

keywords: Marangoni convection; evaporation; pattern formation; amplitude equations

1 Introduction

It is well known that the evaporation of a liquid layer is an endothermic transformation, induces a cooling of the liquid surface and gives rise to a vertical temperature gradient across the liquid layer. As the density and surface tension of the liquid are temperature dependent, this gradient can destabilize the liquid layer: these instabilities are respectively called Rayleigh-Bénard or Marangoni-Bénard instabilities if the temperature dependence of the density or the surface tension is responsible for the onset of convection. The word "Bénard-Marangoni instabilities" is used when both effects combine. Thus, contrary to the classical studies of the Bénard-Marangoni problem (see for example [1]-[6]), in the case of an evaporating liquid layer it is not necessary to impose an external temperature gradient to obtain a destabilization of the system leading to pattern formation. Evaporative convection plays an important role in numerous domains, as for example during drying of paint films, distillation and in heat exchangers. It can also be observed in nature, when the evaporation of a thin layer of water leaves the marks of the convective cells in the clay, or after a salty lake has dried out.

Experimental results on evaporative convection can be found in [7] or in more recent works as [8] and [9].

*Corresponding author, E-mail address: mireille.dondlinger@ulg.ac.be, tel: +32 4 366 33 56 fax: +32 4 366 23 55

Most of the theoretical studies on evaporative convection ([6], [10]-[12]) assume that the liquid layer is in contact only with its own vapor. In this paper we consider in addition the presence of an inert gas in the vapor phase, not only because in most experimental setups the liquid evaporates in a gas (air for example), but also because the presence of a gas strongly stimulates Marangoni-Bénard instabilities, as shown in [13] and [14] (In this case indeed, the temperature perturbations at the interface are related to the variations of the vapor *p*artial pressure instead of being related to the variations of the *t*otal gas pressure). A linear stability analysis of the full two layer system for a liquid evaporating in an inert gas has been carried out in [13] and a deformable free surface was taken into account in [15].

Under certain conditions it is possible to reduce the full two-phase problem to a one-sided model which accounts for the effect of evaporation through a generalized heat transfer condition at the liquid surface, as done in [12], [16], [8], [13] and [14]. A 3D-numerical integration of such a one-sided model was also performed in [17].

The aim of this paper is to perform a weakly nonlinear analysis of the Marangoni instabilities appearing in an evaporating liquid layer surmounted by a vapor-gas mixture on the basis of the one-sided model. This model permits a not too cumbersome derivation of the amplitude equations by a Galerkin-Eckhaus method.

The paper is organized as follows. In section 2 we introduce the physical system, define some dimensionless parameters and establish the basic equations. The reference state and the linear instability threshold of the full two layer problem are determined in sections 3 and 4 respectively. In section 5 we establish the one-sided model and in section 6 we derive the weakly nonlinear amplitude equations from the one-sided problem and we study the stability of the patterns appearing above the linear stability threshold. Conclusions are drawn in section 7.

2 Problem Formulation

We consider an evaporating liquid layer of infinite horizontal extent and depth d_l, surmounted by a gas layer of thickness d_g at a time t_0 (Fig.1). The gas layer is a mixture of the vapor of the liquid and an inert gas.

The lower, rigid and perfectly heat conducting plate is maintained at the temperature T_e. The gas layer is bounded by a perfectly heat conducting upper plate maintained at the same temperature T_e and at constant pressure and concentration. We assume that Boussinesq approximation is valid and that the gas may be taken as perfect. Buoyancy effects are neglected because we assume not too large liquid depths or microgravity conditions. The interface is assumed non deformable so that the moving horizontal liquid-gas interface is described by equation $z = h(t)$. The surface tension σ decreases linearly with the temperature T, i.e.,

$$\sigma = \sigma_0 - \sigma_T(T - T_e)$$

where σ_T is a constant coefficient and T_e the temperature of the bottom and top plates. All other physical properties of the fluids are considered constant and are evaluated at the temperature T_e. The fluid properties were found in [22] and [23].

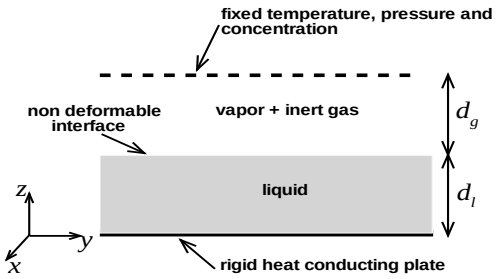

Figure 1: system under study.

The physical properties of the gas mixture are supposed to be those of the inert gas (this is possible provided the mass fraction Y_v of the vapor in the mixture remains sufficiently small). We also suppose that fluctuations in the system evolve much faster than the interface moves i.e. during the stability analysis, the liquid layer thickness does not change. The variables are expressed in dimensionless form: lengths (coordinates (x, y, z)) are scaled by the liquid layer thickness d_l, time t by d_l^2/κ_l, with κ_l the heat diffusivity of the liquid, velocity $\mathbf{V} = (U, V, W)$ by κ_l/d_l (vectors are written in bold characters), pressure P by $\rho_l\kappa_l^2/d_l^2$, with ρ_l the mass density of the liquid, the mass flux J at the interface by $\rho_l\kappa_l/d_l$, temperature T by $L/_{p,l}$ where L is the latent heat of vaporization and $_{p,l}$ the liquid heat capacity per unit mass and the mass fraction of vapor in the gas Y_v by 1 (Y_v is already dimensionless). The dimensionless equations governing the system are standard and given by (subscripts l and g refer to the liquid and gas phases respectively and subscript i refers to the interface):

in the liquid layer:

$$\nabla.\mathbf{V}_l^* = 0 \text{ (continuity)} \tag{1}$$

$$\partial_t\mathbf{V}_l^* + \mathbf{V}_l^*.\nabla\mathbf{V}_l^* + \nabla P_l^* - \mathrm{Pr}_l\nabla^2\mathbf{V}_l^* = 0 \text{ (momentum)} \tag{2}$$

$$\partial_t T_l^* + \mathbf{V}_l^*.\nabla T_l^* - \nabla^2 T_l^* = 0 \text{ (energy)} \tag{3}$$

in the gas layer:

$$\nabla.\mathbf{V}_g^* = 0 \text{ (continuity)} \tag{4}$$

$$\partial_t\mathbf{V}_g^* + \mathbf{V}_g^*.\nabla\mathbf{V}_g^* + \frac{1}{\rho}\nabla P_g^* - \kappa\mathrm{Pr}_g\nabla^2\mathbf{V}_g^* = 0 \text{ (momentum)} \tag{5}$$

$$\partial_t T_g^* + \mathbf{V}_g^*.\nabla T_g^* - \kappa\nabla^2 T_g^* = 0 \text{ (energy)} \tag{6}$$

$$\partial_t Y_v^* + \mathbf{V}_g^*.\nabla Y_v^* - \frac{\kappa}{\mathrm{Le}}\nabla^2 Y_v^* = 0 \text{ (mass diffusion)} \tag{7}$$

where $\mathbf{V}^*$, T^*, P^* and Y_v^* are respectively the dimensionless velocity, temperature, pressure and mass fraction of vapor in the gas. The following definitions are also introduced:

$$\mathrm{Pr}_l = \frac{\nu_l}{\kappa_l} \tag{8}$$

and

$$\mathrm{Pr}_g = \frac{\nu_g}{\kappa_g} \tag{9}$$

are the dimensionless Prandtl numbers in the liquid and in the gas phases respectively and ν_l and ν_g are the cinematic viscosities of the liquid and the gas respectively;

$$\mathrm{Le} = \frac{\kappa_g}{D_g} \tag{10}$$

is the Lewis number, where D_g is the mass diffusivity of the liquid vapor in the gas, $\rho = \rho_g/\rho_l$ and $\kappa = \kappa_g/\kappa_l$.

The boundary conditions at the bottom plate ($z = 0$) express the no-slip condition and the continuity of temperature. These write as:

$$U_l^* = V_l^* = W_l^* = 0; \quad T_l^* = T_e^* \tag{11}$$

At the top ($z = H^*$), one has :

$$\mathbf{V}_g^* = (0, 0, C); \quad T_g^* = T_e^*; \quad Y_v^* = Y_{v,t}^*; \quad P_g^* = P_t^*, \tag{12}$$

where C is a constant with respect to space. Eqs. (12) express that the temperature, pressure and vapor concentration are fixed at the top of the system and that a constant flux of the gas mixture is extracted from the system at $z = H^*$.

At the interface ($z = h^*(t)$):

$$J^* = W_l^* - W_i^* = \rho(W_g^* - W_i^*) \text{ (mass conservation)} \tag{13}$$

$$U_l^* = U_g^*; \quad V_l^* = V_g^* \text{ (no slip condition)} \tag{14}$$

$$\begin{aligned} -\mu(\partial_x W_g^* + \partial_z U_g^*) + \partial_x W_l^* + \partial_z U_l^* + \mathrm{Ma}\partial_x T_l^* = 0 \\ -\mu(\partial_y W_g^* + \partial_z V_g^*) + \partial_y W_l^* + \partial_z V_l^* + \mathrm{Ma}\partial_y T_l^* = 0 \\ \text{(conservation of tangential momentum)} \end{aligned} \tag{15}$$

$$T_l^* = T_g^* = T_i^* \text{ (temperature continuity)} \tag{16}$$

$$J^* - \lambda\partial_z T_g^* + \partial z^* T_l^* = 0 \text{ (energy conservation)} \tag{17}$$

$$J^* = \beta\frac{d_l}{\rho_l\kappa_l}\sqrt{\frac{M_l}{2\Pi R(T_i^*\frac{L}{p,l})}}(p_{sat}(T_i^*\frac{L}{p,l}) - \frac{P_t}{1 + \frac{M_l}{M_g}\frac{1-Y_v^*}{Y_v^*}}) \text{ (Hertz-Knudsen law)} \tag{18}$$

$$\begin{aligned} \frac{\kappa}{\mathrm{Le}}\partial_z Y_v^* + (1 - Y_v^*)(W_g^* - W_i^*) = 0 \\ \text{(non solubility of the gas in the liquid)} \end{aligned} \tag{19}$$

where $H^* = 1 + \frac{d_g}{d_l}$, $W_i = \partial_t h$ is the interface velocity, $Y^*_{v,t}$ and P^*_t are respectively the vapor mass fraction and the pressure at the top plate,

$$\mathrm{Ma} = \frac{\sigma_T d_l L}{c_{p,l}\kappa_l \mu_l} \tag{20}$$

is the Marangoni number, $\mu = \frac{\mu_g}{\mu_l}$ is the ratio of the dynamic viscosity of the gas and the liquid, $\lambda = \frac{\lambda g}{\lambda_l}$ is the ratio of the thermal conductivity of the gas and the liquid, β is the accomodation coefficient, M_l and M_g are the molecular masses of the liquid and the gas respectively, R is the universal gas constant and $p_{sat}(T^*_i \frac{L}{c_{p,l}})$ is the saturation pressure at temperature T_i. Concerning equation (16) we must point out that, strictly speaking, a temperature jump across the interface exists, but it can be neglected as shown in [14]. Recall also that the Hertz-Knudsen law is a phenomenological equation (see for example [6] and [13]) relating the evaporation rate to the difference of the saturation pressure at the interface and the partial pressure of liquid vapor. β represents the probability that a molecule arriving at the interface goes through the interface. In the limit $\beta \to \infty$, equation (18) is equivalent to the Clausius-Clapeyron relation and the liquid-gas interface is at thermodynamic equilibrium (i.e. there is no resistance to phase transition at the interface).

3 Reference state

We work in the quasi-steady assumption [12] which means that close to the time t_0, the time scale of the interface displacement is much larger than the time scale of heat and mass diffusion. This assumption is possible thanks to the large value of the latent heat of vaporization L leading to low evaporation rates (this can be seen through the dimensional form of equation (17) which writes as: $JL - \lambda_g \partial_z T_g + \lambda_l \partial z T_l = 0$) and thus slow interface displacements. Within this assumption the above system admits a solution without horizontal flow, where the velocity, thermal and concentration fields depend only on the vertical coordinate and where the time derivatives can be neglected in the partial differential equations. This is our reference state. It is given by (subscript ref refers to the reference state):

$$\mathbf{V}^*_{ref,\,l} = (0,0,0) \tag{21}$$

$$\mathbf{V}^*_{ref,\,g} = (0,0,J^*_{ref}(\frac{1}{\rho}-1)) \simeq (0,0,\frac{J^*_{ref}}{\rho}) \tag{22}$$

$$T^*_{ref,\,l} = (T^*_{ref,\,i} - T^*_e)z + T^*_e \tag{23}$$

$$T^*_{ref,\,g} = \frac{(T^*_{ref,\,i} - T^*_e)e^{\frac{J^*_{ref}(z-1)}{\rho\kappa}} + T^*_e - T^*_{ref,\,i} e^{\frac{J^*_{ref}(H^*-1)}{\rho\kappa}}}{1 - e^{\frac{J^*_{ref}(H^*-1)}{\rho\kappa}}} \tag{24}$$

$$Y^*_{v,ref} = -(1 - Y^*_{v,t})e^{\frac{J^*_{ref}\mathrm{Le}(z-H^*)}{\rho\kappa}} + 1 \tag{25}$$

where J^*_{ref} and $T^*_{ref,\,i}$ must be determined numerically by solving the following system of equations involving the three unknown quantities J^*_{ref}, $T^*_{ref,\,i}$ and

$Y_{v,ref,i}$:

$$J^*_{ref} = \frac{\lambda(T^*_{ref,\,i} - T^*_e)J^*_{ref}}{(1 - e^{\frac{J^*_{ref}(H^*-1)}{\rho\kappa}})\rho\kappa} - T^*_{ref,\,i} + T^*_e \tag{26}$$

$$J^*_{ref} = \frac{\beta d_l}{\rho_l \kappa_l}\sqrt{\frac{M_l}{2\pi R(T^*_{ref,\,i}\frac{L}{c_{p,l}})}}(p_{sat}(T^*_{ref,\,i}\frac{L}{c_{p,l}}) - \frac{P_t}{1 + \frac{M_l}{M_g}\frac{1-Y^*_{v,ref,i}}{Y^*_{v,ref,i}}}) \tag{27}$$

$$J^*_{ref} = \frac{\rho\kappa}{\mathrm{Le}(1-H^*)} ln(\frac{Y^*_{v,ref,i} - 1}{Y^*_{v,t} - 1}) \tag{28}$$

Some reference temperature, mass fraction of vapor in the gas and velocity profiles are given in figures (2-5).

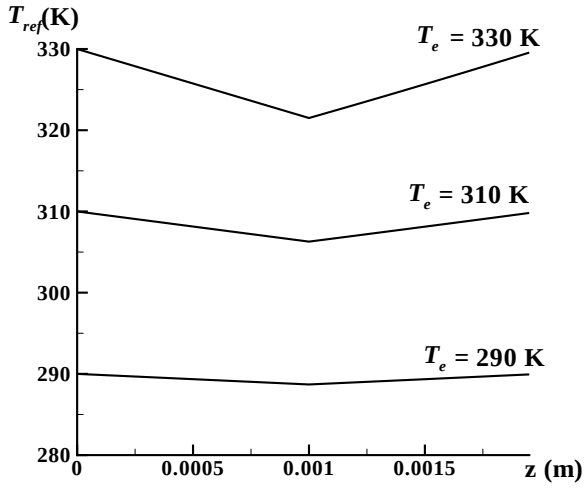

Figure 2: reference temperature profiles for water($\beta = 0.01$, $Y_{v,t} = 0$, $P_t = 1$ atm, $d_l = d_g = 0.001$ m).

In the next section we will analyse the stability of this reference state.

4 Linear stability analysis

To determine the stability of the reference state at time t_0, we introduce small perturbations for velocity, temperature, pressure and vapor mass fraction:

$$\mathbf{V}^* = \mathbf{V}^*_{ref} + \mathbf{v}' \tag{29}$$

$$T^* = T^*_{ref} + \theta' \tag{30}$$

$$P^* = P^*_{ref} + \pi' \tag{31}$$

in the liquid and gas phase and

$$Y^*_v = Y^*_{v,ref} + y'_v \tag{32}$$

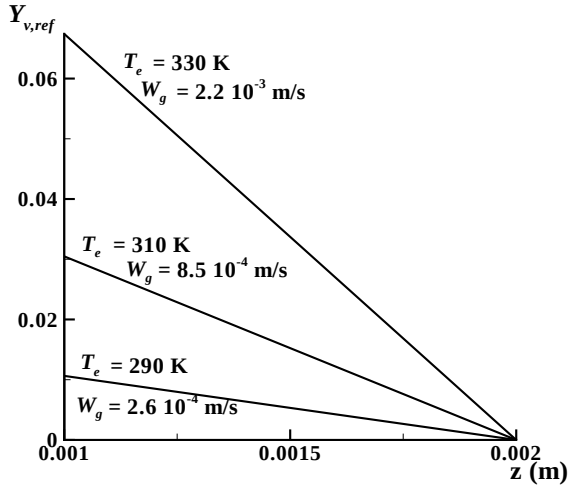

Figure 3: reference mass fraction of vapor in the gas and vertical velocity for water($\beta = 0.01$, $Y_{v,t} = 0$, $P_t = 1$ atm, $d_l = d_g = 0.001$ m).

After linearization of the equations governing the perturbations, the pressure field π' is eliminated by applying $\nabla \times \nabla \times$ to the momentum equation. Then, the velocity, temperature and vapor mass fraction perturbations are written as plane waves (normal modes) of the form:

$$(w', \theta', y'_v) = (w(z), \theta(z), y_v(z)) e^{i(k_x x + k_y y)} e^{\sigma t} \tag{33}$$

where σ is the complex growth rate of the perturbations and k_x and k_y are the components of the horizontal wave vector $\mathbf{k}$. After standard algebraic calculations, we find the following equations:

for $0 \leq z \leq 1$:

$$\sigma(D^2 - k^2)w_l - \mathrm{Pr}_l(D^4 - 2k^2D^2 + k^4)w_l = 0 \tag{34}$$

$$\sigma\theta - (D^2 - k^2)\theta_l + (T^*_{ref,i} - T^*_e)w_l = 0 \tag{35}$$

for $1 \leq z \leq H^*$:

$$\sigma(D^2 - k^2)w_g + (-\mathrm{Pr}_g\kappa(D^4 - k^2D^2 + k^4) + \frac{J^*_{ref}}{\rho}(D^3 - k^2D))w_g = 0 \tag{36}$$

$$\sigma\theta_g + (-D^2 + \frac{J^*_{ref}}{\rho}D + \kappa k^2)\theta_g + \frac{(T^*_{ref,i} - T^*_e)J^*_{ref} e^{\frac{J^*_{ref}(z-1)}{\rho\kappa}}}{\rho\kappa(1 - e^{\frac{J^*_{ref}(H^*-1)}{\rho\kappa}})} w_g = 0 \tag{37}$$

$$\sigma\, y_v + (-\frac{\kappa}{\mathrm{Le}}D^2 + \frac{J^*_{ref}}{\rho}D + \frac{\kappa k^2}{\mathrm{Le}})y_v - (1 - Y^*_{v,t})\frac{J^*_{ref}\mathrm{Le}}{\rho\kappa} e^{\frac{J^*_{ref}\mathrm{Le}(z-H^*)}{\rho\kappa}} w_g = 0 \tag{38}$$

at $z = 0$:

$$w_l = Dw_l = \theta_l = 0 \tag{39}$$

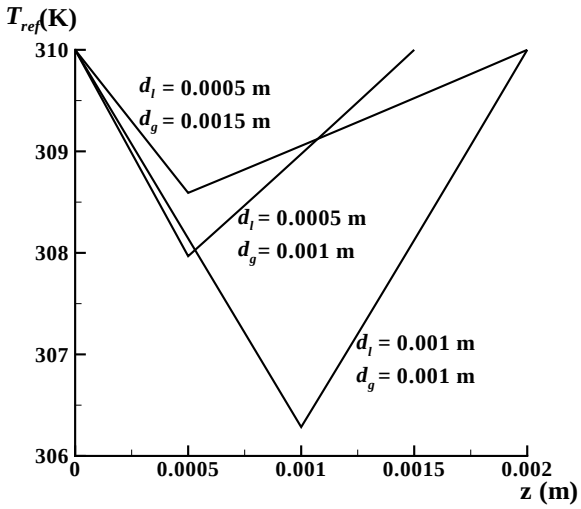

Figure 4: reference temperature profiles for water ($\beta = 0.01$, $Y_{v,t} = 0$, $P_t = 1$ atm, $T_e = 310$ K).

at $z = H^*$:

$$w_g = Dw_g = \theta_g = y_v = 0 \tag{40}$$

at $z = 1$:

$$w_l = \rho w_g = 0 \tag{41}$$

$$Dw_l - Dw_g = 0 \tag{42}$$

$$\mu(D^2 + k^2)w_g - (D^2 + k^2)w_l - k^2 \mathrm{Ma}\theta_l = 0 \tag{43}$$

$$\theta_l - \theta_g = 0 \tag{44}$$

$$w_l - \lambda D\theta_g + D\theta_l = 0 \tag{45}$$

$$w_l - \frac{\partial f}{\partial T_l^*} \mid_{ref} \theta_l - \frac{\partial f}{\partial Y_v^*} \mid_{ref} y_v = 0 \tag{46}$$

$$(\frac{\kappa}{\mathrm{Le}} D - J_{ref}^*((1 + \frac{1}{\rho}))y_v + (1 - Y_{v,t}^*)e^{\frac{J_{ref}^* \mathrm{Le}(1-H^*)}{\rho\kappa}} w_g = 0 \tag{47}$$

where $D = \partial_z$ and

$$f(T_l^*, Y_v^*) = \beta \frac{d_l}{\rho_l \kappa_l} \sqrt{\frac{M_l}{2\Pi R(T_l^* \frac{L}{c_{p,l}})}} (p_{sat}(T_l^* \frac{L}{c_{p,l}}) - \frac{P_t}{1 + \frac{M_l}{M_g} \frac{1 - Y_v^*}{Y_v^*}}) \tag{48}$$

To solve the problem, we decompose $w(z)$, $\theta(z)$ and $y_v(z)$ in series of Chebyshev polynomials (spectral Tau-Chebyshev method). Then after projection of the equations on the Chebyshev polynomials and taking their orthogonality properties into account the final set of equations and boundary conditions (34-48) can be written in the general form of an algebraic eigenvalue problem:

$$A\mathbf{X} = \sigma B\mathbf{X} \tag{49}$$

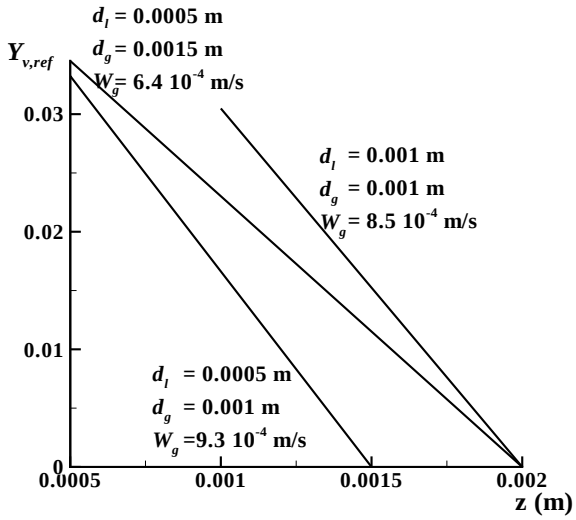

Figure 5: reference mass fraction of vapor in the gas and vertical velocity for water($\beta = 0.01$, $Y_{v,t} = 0$, $P_t = 1$ atm, $T_e = 310$ K).

where A and B are two matrices depending on the parameters of the problem and $\mathbf{X}$ is the vector of the unknown coefficients of the series. The marginal stability curve is defined by $\mathrm{Re}(\sigma) = 0$. For given liquid and gas and for fixed values of parameters P_t, $Y_{v,t}$, T_e, d_g and d_l we can calculate the value of one of these parameters, for which $\mathrm{Re}(\sigma) = 0$, as a function of the others and of the wave number k. For the linear stability results we choose d_l as the bifurcation parameter (as in most of the studies on evaporative convection).

Figs 6 and 7 (full curves) represent the marginal stability curves obtained in the case where the liquid is water and the gas is air and for different values of T_e and d_g. Note that the liquid depth is given in dimensional units because lengths have been scaled by d_l. The results in the case of an ethanol-air system are represented in Fig. 8.

Note also that we checked that the exchange of stability ($\mathrm{Re}(\sigma) = 0 \Rightarrow \mathrm{Im}(\sigma) = 0$) is verified in the cases studied here (we did not impose $\mathrm{Im}(\sigma) = 0$ a priori, as it is often done).

The results are independent of β for values of $\beta \geq 0.01$ and change very little for lower values of β (contrary to the case of a liquid-vapor system without gas, [18]), i.e. the gas-liquid interface is very close to local thermodynamic equilibrium.

The critical value of the parameter d_l is defined by:

$$d_{l,\,c} = \min_k d_l \tag{50}$$

The wave number corresponding to $d_{l,c}$ is the critical wave number k_c. Some critical values can be found in table 1.

Note that for standard temperatures, the critical liquid depth is very low, which means that "usual" liquid layers are always unstable.

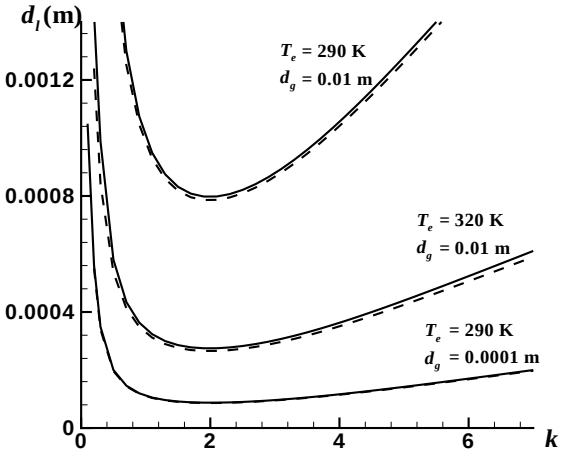

Figure 6: Marginal stability curves for water ($\beta = 0.01$, $Y_{v,t} = 0$, $P_t = 1$ atm). Full lines: exact two layer problem, dashed lines: one-sided model.

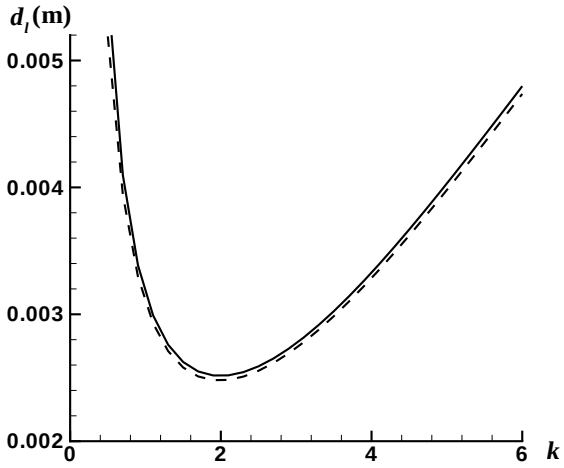

Figure 7: Marginal stability curves for water ($\beta = 0.01$, $Y_{v,t} = 0$, $P_t = 1$ atm, $T_e = 290$ K, $d_g = 0.1$ m). Full lines: exact two layer problem, dashed lines: one-sided model.

5 One-sided model

As a basis for the nonlinear stability analysis of the next section, we first reduce the system to a one-sided model, which allows to solve the equations in the liquid phase only, but takes into account relevant effects in the gas phase through

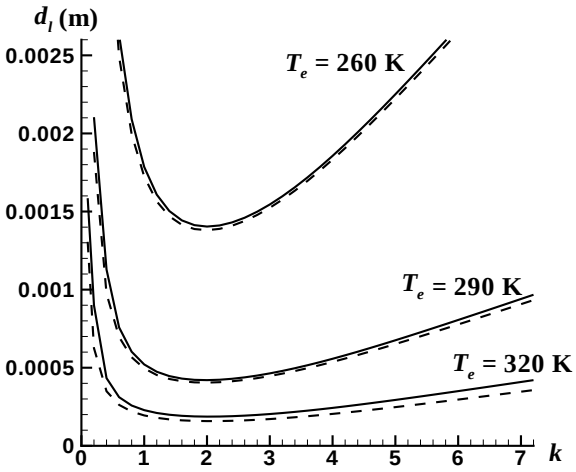

Figure 8: Marginal stability curves for ethanol ($\beta = 0.01$, $Y_{v,t} = 0$, $P_t = 1$ atm, $d_g = 0.01$ m). Full lines: exact two layer problem, dashed lines: one-sided model.

Table 1: $d_{l,c}$, k_c, J and relative errors $\epsilon_{d_{l,c}} = \frac{d_{l,c,one-sided} - d_{l,c}}{d_{l,c}}$ and $\epsilon_{k_c} = \frac{k_{c,one-sided} - k_c}{k_c}$

liquid	T_e(m)	d_g(m)	$d_{l,c}$(m)	k_c	J(kg/m^{2}s)	$\epsilon_{d_{l,c}}$	ϵ_{k_c}
water	290	0.0001	8.74E-05	2.006	2.8E-03	-1.24E-02	-2.28E-04
water	290	0.01	7.97E-04	1.995	3.0E-5	-1.47E-02	-2.80E-03
water	290	0.1	2.51E-03	1.995	3.5E-6	-1.44E-02	-4.07E-03
water	320	0.01	2.75E-04	1.992	2.1E-4	-3.34E-02	3.99E-05
ethanol	260	0.01	1.40E-03	2.013	2.1E-5	-1.63E-02	-1.01E-02
ethanol	290	0.01	4.21E-04	1.988	1.5E-4	-3.77E-02	-5.54E-03
ethanol	320	0.01	1.87E-04	2.038	1.1E-3	-1.54E-01	1.51E-02

boundary conditions (details on the derivation of the one-sided model can be found for example in [8], [13] and [14]). This reduction is possible, provided the depth of the gas is not too large and transport effects in the gas are negligible ($1/\kappa << 1$ and $\mathrm{Le}/\kappa << 1$) so that equations (6-7) reduce to:
($1 \leq z \leq H^*$),

$$\nabla^2 T_g^* = 0 \tag{51}$$

$$\nabla^2 Y_v^* = 0 \tag{52}$$

Assuming furthermore that the evaporation rate is not too high, the reference state is given by:

$$\mathbf{V}_{ref,l}^* = (0, 0, 0) \tag{53}$$

$$\mathbf{V}^*_{ref,g} = (0, 0, \frac{J^*_{ref}}{\rho}) \tag{54}$$

$$T^*_{ref,\,l} = (T^*_{ref,i} - T^*_e)z + T^*_e \tag{55}$$

$$T^*_{ref,\,g} = \frac{(T^*_{ref,i} - T^*_e)}{1 - H^*}z + T^*_e - \frac{T^*_{ref,\,i} - T^*_e}{1 - H^*}H^* \tag{56}$$

$$Y^*_{v,ref} = \frac{J^*_{ref}(-1 + Y^*_{v,t})}{\frac{\rho\kappa}{Le} - d^*_l J^*_{ref} + H^* J^*_{ref}}(z - H^*) + Y^*_{v,t} \tag{57}$$

As J^*_{ref}, $T^*_{ref,\,i}$ and $Y^*_{v,ref,\,i}$ are rather complicated expressions, they are given herebelow in the case where $Y^*_{v,t} = 0$.

$$J^*_{ref} = \frac{d_l}{\rho_l \kappa_l} \frac{p_{sat}(T_e)}{\frac{\partial p_{sat}}{\partial T}|_{T_e}\frac{L d_l}{\lambda_l} + \frac{1}{\beta\sqrt{\frac{M_l c_{p,l}}{2\Pi R L T^*_e}}}(1 + \frac{\lambda}{d^*_g}) + \frac{R d_g L T^*_e}{M_l D_g c_{p,l}}} \tag{58}$$

$$T^*_{ref,\,i} = T^*_e - \frac{J^*_{ref}}{1 + \frac{\lambda}{d^*_g}} \tag{59}$$

$$Y^*_{v,ref,\,i} = \frac{d^*_g \mathrm{Le}}{\rho\kappa} J^*_{ref} \tag{60}$$

The expression for J^*_{ref} shows clearly the three possible limitating mechanisms of the evaporation process: the first term of the denominator is the resistance to heat supply to the interface, the second one the resistance to phase transition and the third one is resistance to vapor removal by diffusion. For a detailed discussion of the relative importance of these mechanisms see the paper [13]. In general the second term is much smaller than the other two ones; this means that the interface is very close to local thermodynamic equilibrium.

After introduction of the perturbed quantities, as in section 4, in eqs. (1-3) and in eqs. (51- 52), we obtain the following linear equations governing the system (in the following we drop the subscript l of the variables): for $\leq z \leq 1$:

$$\sigma(D^2 - k^2)w - \mathrm{Pr}_l(D^4 - 2k^2D^2 + k^4)w = 0, \tag{61}$$

$$\sigma\theta - (D^2 - k^2)\theta + (T^*_{ref,\,i} - T^*_e)w = 0, \tag{62}$$

and at $z = 0$:

$$w = Dw = \theta = 0, \tag{63}$$

$$w = (D^2 + k^2)w + \mathrm{Ma}k^2\theta = D\theta + (\mathrm{Bi}_{ev} + \lambda k coth((1 - H^*)k))\theta = 0. \tag{64}$$

where Bi_{ev}, that takes account for the effect of evaporation, is a rather complicated expression depending on the wave number k, the liquid and gas properties and the reference state. The expression of Bi_{ev} when $Y^*_{v,t} = 0$ is given herebelow:

$$\mathrm{Bi}_{ev} = \frac{\frac{L}{c_{p,l}}\frac{\partial p_{sat}}{\partial T}|_{T_{i,ref}} - \frac{J^*_{ref}\rho_l\kappa_l}{2\beta d_l T^*_{ref,i}\sqrt{\frac{M_l c_{p,l}}{2\Pi R L T^*_{ref,i}}}}}{\frac{\rho_l\kappa_l}{\beta d_l\sqrt{\frac{M_l c_{p,l}}{2\Pi R L T^*_{ref,i}}}} + \frac{\frac{M_l}{M_g}(1 - Y^*_{v,ref,i})P_t}{(\frac{M_l}{M_g} + (1 - \frac{M_l}{M_g})Y^*_{v,ref,i})^2(\frac{\rho\kappa}{\mathrm{Le}}k coth(k(H^* - 1)) + J^*_{ref})}} \tag{65}$$

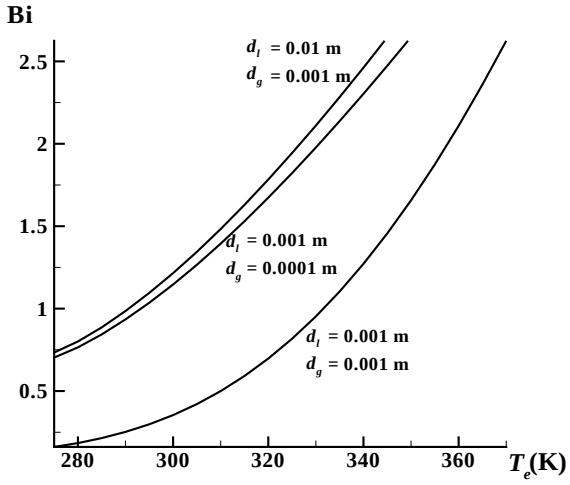

Figure 9: Biot number Bi=$\text{Bi}_{ev} + \lambda k coth((1 - H^*)k)$ for water as a function of temperature T_e ($\beta = 0.01$, $Y_{v,t} = 0$, $P_t = 1$ atm).

In figures (9-11), we plotted the Biot number (evaluated at $k = 2$) as a function of T_e, d_l and d_g respectively.

Contrary to ([17], eq. (18)), the equivalent Biot number depends on the wavenumber k because the evaporation rate is obtained here by the resolution of the diffusion equation (52) associated with the saturation equation (19) instead of being given by a measured function of the interface temperature.

We have thus transformed the initial two-layer problem (34-48) in a one-sided model (61-64), that is similar to the classical Pearson problem [3]. The marginal stability curves corresponding to this problem, are obtained by a linear stability analysis as in section 4. In Figs. 6, 7 and 8 we compare these curves to those obtained from the exact two layer problem. One can see that there is a very good agreement between the two approaches and that it is best when T_e and d_g are low. This is due to the fact that when T_e increases, the evaporation rate increases and the one-sided model was established under the hypothesis of low evaporation rates. We assumed in the one-sided model that transport effects in the gas are negligible, which is valid only for low values of d_g. Nevertheless we see in Fig. 7 that even for values of d_g as high as 0.1 m (compared to the liquid layer thickness), there is a rather good agreement between the two approaches. In table 1 we see the relative error for some critical values.

6 Nonlinear stability analysis

The linear analysis allowed us to determine the critical liquid depth $d_{l,c}$ above which the reference state becomes unstable, as well as the characteristic wave number k_c of the flow pattern. But the actual shape of this pattern can be obtained only via a nonlinear analysis. For this purpose, we use a Galerkin-Eckhaus method, which consists in expanding the unknown perturbation fields

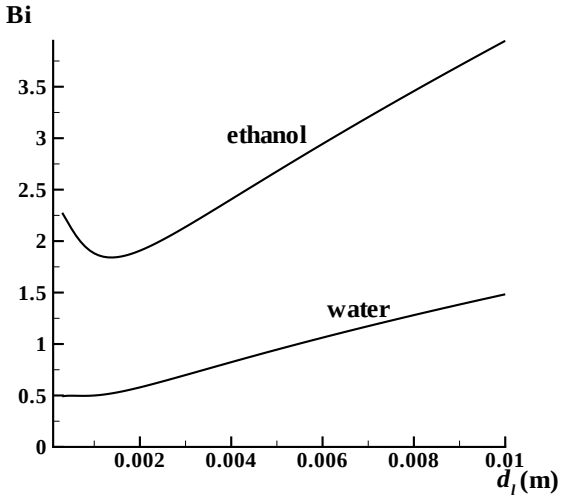

Figure 10: Biot number Bi=$\mathrm{Bi}_{ev} + \lambda k coth((1 - H^*)k)$ as a function of d_l ($\beta = 0.01$, $Y_{v,t} = 0$, $P_t = 1$ atm, $T_e = 310$ K, $d_g = 0.001$ m).

in series of the eigenfunctions of the linear problem, then to introduce these expansions in the nonlinear equations and to project them onto the eigenfunctions of the adjoint linear problem. The infinite set of equations is then reduced to a finite number of ordinary differential equations by using a slaving principle.

In order to avoid too complicated calculations, we consider the one-sided model derived in section 5 (with a constant Biot number evaluated at the critical liquid depth). The nonlinear perturbed equations for this one-sided model are given by:

for $0 \leq z \leq 1$:

$$\nabla^*.\mathbf{v}' = 0 \tag{66}$$

$$\partial_t \mathbf{v}' + \mathbf{v}'.\nabla \mathbf{v}' + \nabla^* \pi' - \mathrm{Pr}_l \nabla^2 \mathbf{v}' = 0 \tag{67}$$

$$\partial_t \theta' + \mathbf{v}'.\nabla \theta' + (T^*_{ref,\,i} - T^*_e) w' - \nabla^2 \theta' = 0 \tag{68}$$

$$\tag{69}$$

at $z = 0$:

$$\mathbf{v}' = \theta' = 0 \tag{70}$$

at $z = 1$:

$$w' = 0 \tag{71}$$

$$\partial_x w' + \partial_z u' = -\mathrm{Ma} \partial_x \theta'$$

$$\partial_y w' + \partial_z v' = -\mathrm{Ma} \partial_y \theta' \tag{72}$$

$$\partial_z \theta' = -(\mathrm{Bi}_{ev} + \lambda k_c coth(d^*_g k_c))\theta' \tag{73}$$

For conciseness the derivation of the amplitude equations is described only briefly in the present paper. For further details see for instance [19] or [20].

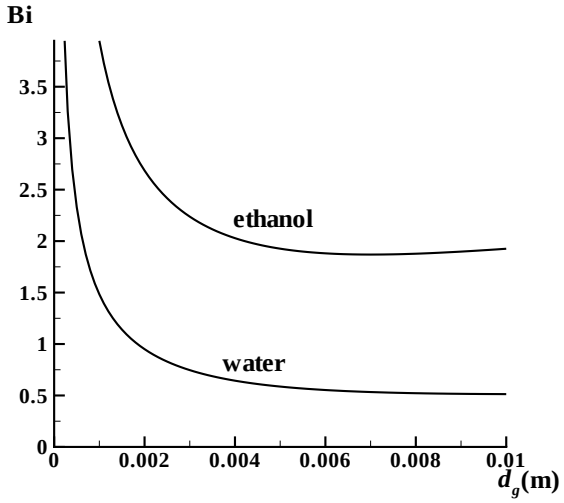

Figure 11: Biot number Bi=Bi$_{ev}$ + $\lambda k coth((1-H^*)k)$ as a function of d_g ($\beta = 0.01$, $Y_{v,t} = 0$, $P_t = 1$ atm, $T_e = 310$ K, $d_l = 0.01$ m).

First we solve the linear equations (61)-(64) using the growth rate σ of the perturbations as eigenvalue parameter. For each value of the wave number k there exists an infinite set of eigenvalues σ_p^k, with p being an integer running from one to infinity. The unknowns of the nonlinear problem (66)-(73) are then expanded as a series of the eigenfunctions $(\mathbf{v}_p^{\mathbf{k}}(z), \theta_p^{\mathbf{k}}(z))$ of the linear eigenvalue problem:

$$(\mathbf{v}', \theta') = \sum_{p=1}^{\infty} \sum_{\mathbf{k}} A_p^{\mathbf{k}}(t)(\mathbf{v}_p^{\mathbf{k}}(z), \theta_p^{\mathbf{k}}(z)) e^{i(k_x x + k_y y)} \tag{74}$$

$A_p^{\mathbf{k}}$ are the time-dependent amplitudes and $\mathbf{k}$ can take all possible directions and moduli. After inserting equation (74) in the nonlinear equations, projection onto the eigenfunctions of the adjoint problem, integration by parts and noticing that the eigenfuctions are biorthogonal we obtain an infinite set of amplitude equations. This set is then reduced to a finite number by using a slaving method. The principle of this method consists in separating the set of eigenmodes in a first set K_c, containing the most unstable (critical) modes, and a second set K_s, containing the stable (slaved) modes. The final amplitude equations are then given by:

$$\begin{aligned} \partial_t^* \quad A_p^{\mathbf{k}} = \quad \sigma_p^{\mathbf{k}} A_p^{\mathbf{k}} + \varepsilon \quad \sum_{\substack{q \\ A_q^{\mathbf{k}} \in K_c}} M_{q,p}^{\mathbf{k}} A_q^{\mathbf{k}} - \quad \sum_{\substack{q, l, \mathbf{k}_1, \mathbf{k}_2 \\ A_q^{\mathbf{k}_1}, A_l^{\mathbf{k}_2} \in K_c}} N_{q,l,p}^{\mathbf{k}_1, \mathbf{k}_2, \mathbf{k}} A_q^{\mathbf{k}_1} A_l^{\mathbf{k}_2} \\ - \quad \sum_{\substack{q, m, n, \mathbf{k}_1, \mathbf{k}_3, \mathbf{k}_4 \\ A_q^{\mathbf{k}_1}, A_m^{\mathbf{k}_3}, A_n^{\mathbf{k}_4} \in K_c}} Z_{q,m,n,p}^{\mathbf{k}_1, \mathbf{k}_3, \mathbf{k}_4, \mathbf{k}} A_q^{\mathbf{k}_1} A_m^{\mathbf{k}_3} A_n^{\mathbf{k}_4} \end{aligned} \tag{75}$$

where

$$M_{q,p}^{\mathbf{k}} = -T_{e,c}\left\langle \mathbf{v}_p^{\mathbf{k}\star}\mathbf{v}_p^{\mathbf{k}} + \theta_p^{\mathbf{k}\star}\theta_p^{\mathbf{k}}\right\rangle^{-1}\Big(\frac{\partial(T_{ref,i}^* - T_e^*)}{\partial T_e}\mid_{T_{e,c}}\left\langle w_p^{\mathbf{k}}, \theta_q^{\mathbf{k}\star}\right\rangle$$
$$-\frac{\partial \mathrm{Pr}_l}{\partial T_e}\mid_{T_{e,c}}\left\langle \nabla^2\mathbf{v}_p^{\mathbf{k}}, \mathbf{v}_q^{\mathbf{k}\star}\right\rangle + \mathrm{Pr}_l\frac{\partial Ma}{\partial T_e}\mid_{T_{e,c}}\left\langle \nabla_h\theta_p^{\mathbf{k}}, \mathbf{v}_q^{\mathbf{k}\star}\right\rangle_{z=1}$$
$$+(\frac{\partial \mathrm{Bi}_{ev}}{\partial T_e}\mid_{T_{e,c}} + \frac{\partial \lambda}{\partial T_e}\mid_{T_{e,c}} k_c coth(d_g^* k_c))\left\langle \theta_p^{\mathbf{k}}, \theta_q^{\mathbf{k}\star}\right\rangle_{z=1}\Big)$$

$$N_{q,l,p}^{\mathbf{k}_1,\mathbf{k}_2,\mathbf{k}} = \frac{\left\langle \mathbf{v}_q^{\mathbf{k}_1}.\nabla\mathbf{v}_l^{\mathbf{k}_2}, \mathbf{v}_p^{\mathbf{k}\star}\right\rangle + \left\langle \mathbf{v}_q^{\mathbf{k}_1}.\nabla\theta_l^{\mathbf{k}_2}, \theta_p^{\mathbf{k}\star}\right\rangle}{\left\langle \mathbf{v}_p^{\mathbf{k}}\mathbf{v}_p^{\mathbf{k}\star} + \theta_p^{\mathbf{k}}\theta_p^{\mathbf{k}\star}\right\rangle}$$

$$Z_{q,m,n,p}^{\mathbf{k}_1,\mathbf{k}_3,\mathbf{k}_4,\mathbf{k}} = -\sum_{\substack{r,\mathbf{k}_5 \\ A_r^{\mathbf{k}_5}\in K_c}}(N_{q,r,p}^{\mathbf{k}_1,\mathbf{k}_5,\mathbf{k}} + N_{r,q,p}^{\mathbf{k}_5,\mathbf{k}_1,\mathbf{k}})N_{m,n,r}^{\mathbf{k}_3,\mathbf{k}_4,\mathbf{k}_5} \times\frac{1}{iIm(\sigma_m^{\mathbf{k}_3} + \sigma_n^{\mathbf{k}_4}) - \sigma_r^{\mathbf{k}_5}}$$

$\varepsilon = (T_e - T_{e,\,c})/(T_{e,\,c})$ is the relative distance to the linear stability threshold. Note that we choose this definition for ε (and not $(d_l - d_{l,c})/d_{l,c}$) because the expression of $M_{q,p}^{\mathbf{k}}$ is less complicated in this case. The final stability diagrams are the same in both cases. The scalar products $\langle \quad , \quad \rangle$ are defined by:

$$\langle a, b\rangle = \lim_{L\to\infty}\frac{1}{4L^2}\int_{-L}^{L}\int_{-L}^{L}\int_{0}^{1} a(x,y,z)\ \bar{b}(x,y,z)\ dz\ dx\ dy \tag{76}$$

and

$$\langle a, b\rangle_{z=1} = \lim_{L\to\infty}\frac{1}{4L^2}\int_{-L}^{L}\int_{-L}^{L} a(x,y,1)\ \bar{b}(x,y,1)\ dx\ dy \tag{77}$$

Note that in equation (75), contrary to what is usually done, we take into account the variation of the physical parameters and of the Biot number with $T_{e,ref}$ (but in agreement with Boussinesq approximation the variation of the physical parameters with the small temperature perturbations θ are neglected).

In order to describe the interactions of roll, square and hexagonal patterns, we choose 12 critical wave vectors with an angle of 30° between them (see figure 12).

In this case the final amplitude equations are of the form (to simplify notation we note $A_1^{\mathbf{k}_1} = A_1, A_1^{\mathbf{k}_2} = A_2 ...$):

$$\tau\partial_t A_1 = \varepsilon A_1 + a\overline{A}_2\overline{A}_3 - b(|A_2|^2 + |A_3|^2)A_1 - c|A_1|^2 A_1$$
$$-d(|A_5|^2 + |A_6|^2)A_1 - e|A_4|^2 A_1 \tag{78}$$

and similar equations for $A_2 ... A_{12}$ (see [21]). The coefficients τ, a, b, c, d and e are given by:

$$\tau \quad = \quad \frac{1}{M_{1,1}^{\mathbf{k}_1}},$$

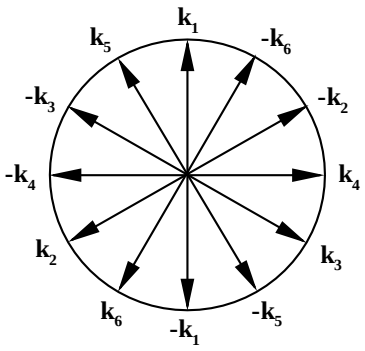

Figure 12: critical wave vectors

$$
\begin{aligned}
a &= \tau\, N_{1,1,1}^{-\mathbf{k}_2,-\mathbf{k}_3,\mathbf{k}_1}, \\
b &= \tau\, Z_{1,1,1,1}^{\mathbf{k}_1,\mathbf{k}_2,-\mathbf{k}_2,\mathbf{k}_1} = \tau\, Z_{1,1,1,1}^{\mathbf{k}_1,\mathbf{k}_3,-\mathbf{k}_3,\mathbf{k}_1}, \\
c &= \tau\, Z_{1,1,1,1}^{\mathbf{k}_1,\mathbf{k}_1,-\mathbf{k}_1,\mathbf{k}_1}, \\
d &= \tau\, Z_{1,1,1,1}^{\mathbf{k}_1,\mathbf{k}_5,-\mathbf{k}_5,\mathbf{k}_1} = \tau\, Z_{1,1,1,1}^{\mathbf{k}_1,\mathbf{k}_6,-\mathbf{k}_6,\mathbf{k}_1}, \\
e &= \tau\, Z_{1,1,1,1}^{\mathbf{k}_1,\mathbf{k}_4,-\mathbf{k}_4,\mathbf{k}_1}
\end{aligned}
$$

A standard stability analysis of the solutions of these amplitude equations shows that:

- the conductive solution is stable when $\varepsilon < 0$
- rolls are stable when $c > 0$ and $c < b$ and $c < d$ and $c < e$ and $\varepsilon > \varepsilon_R$
- hexagons are stable when $\varepsilon > \varepsilon_{Hc}$ and $2b + c > 0$ and

  $$\left(\begin{array}{l} c > b \text{ or} \\ (-b < c < b \text{ and } \varepsilon < \varepsilon_{H1}) \end{array} \right) \text{ and}$$

  $$\left(\begin{array}{l} 2d + e > 2b + c \text{ or} \\ (-(2b + c) < 2d + e < 2b + c \text{ and } \varepsilon < \varepsilon_{H2}) \end{array} \right)$$
- squares are stable when $c + e > 0$ and $c > e$ and $c + e - b - d < 0$ and $\varepsilon > \varepsilon_S$

where

$$\varepsilon_R = \frac{c\,a^2}{(b-c)^2},\ \varepsilon_{Hc} = \frac{-a^2}{4(2b+c)},\ \varepsilon_{H1} = \frac{a^2(b+2c)}{(b-c)^2},$$

$$\varepsilon_{H2} = \frac{a^2(2d+e)}{(2d+e-2b-c)^2}, \varepsilon_S = \frac{a^2(c+e)}{(b+d-c-e)}$$

In Figs. 13 and 14 we see the results of this stability analysis in the case of a water-air system and for two different values of the gas layer thickness (respectively 0.01 m and 0.0001 m); C means that the conductive state is stable, R means that rolls are a stable pattern, H means that hexagons are a stable pattern and S means that squares are a stable pattern.

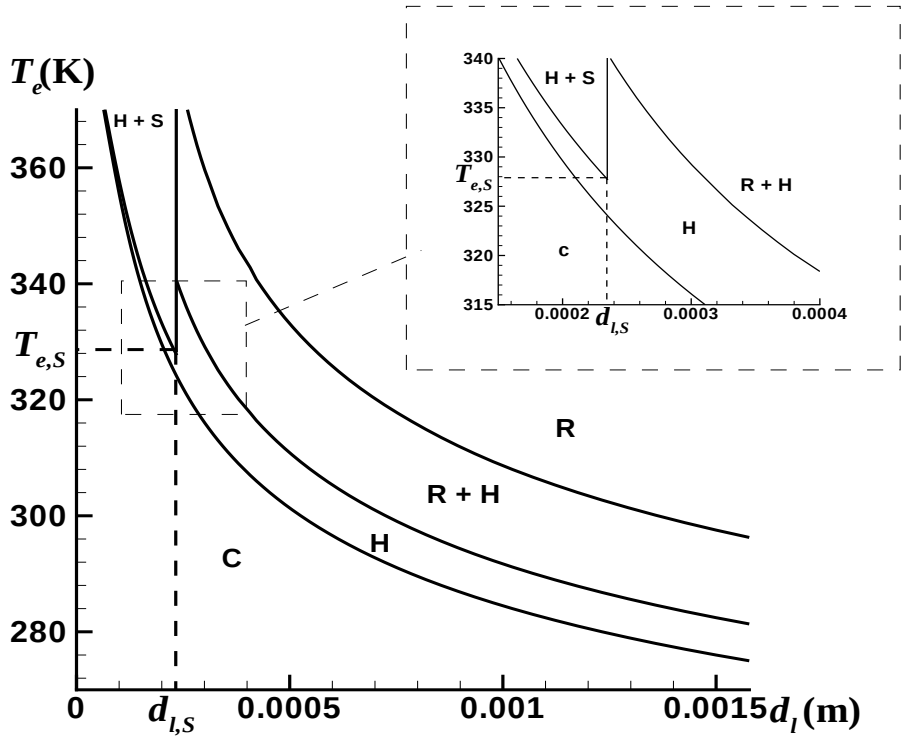

Figure 13: weakly nonlinear stability diagram for water ($\beta = 0.01$, $Y_{v,t} = 0$, $P_t = 1$ atm, $d_g = 0.01$ m).

Fig. 14 shows that for a very thin gas layer square structures will not be observed. In figure 15 we present the liquid depth $d_{l,S}$ below which squares are possible as a function of d_g. Corresponding temperatures $T_{e,S}$ above which squares are stable are also indicated. For a better comprehension of the definition of $d_{l,S}$ and $T_{e,S}$, they are indicated in figure 13.

In figure 16 we see the results of the stability analysis for an ethanol-air system. This liquid was analysed because it is the fluid used in the ITEL-MASER 9 experiment (see [8]). The results of this experiment are not comparable to our theoretical results because they observed only transient effects due to the short experiment duration, but experiments with longer experiment times (and thus pattern formation) are foreseen in the CIMEX-1 experiment ([8]).

We thus see that the details of the nonlinear stability diagrams depend on the fluid and the experimental conditions (through d_g for instance), but as a

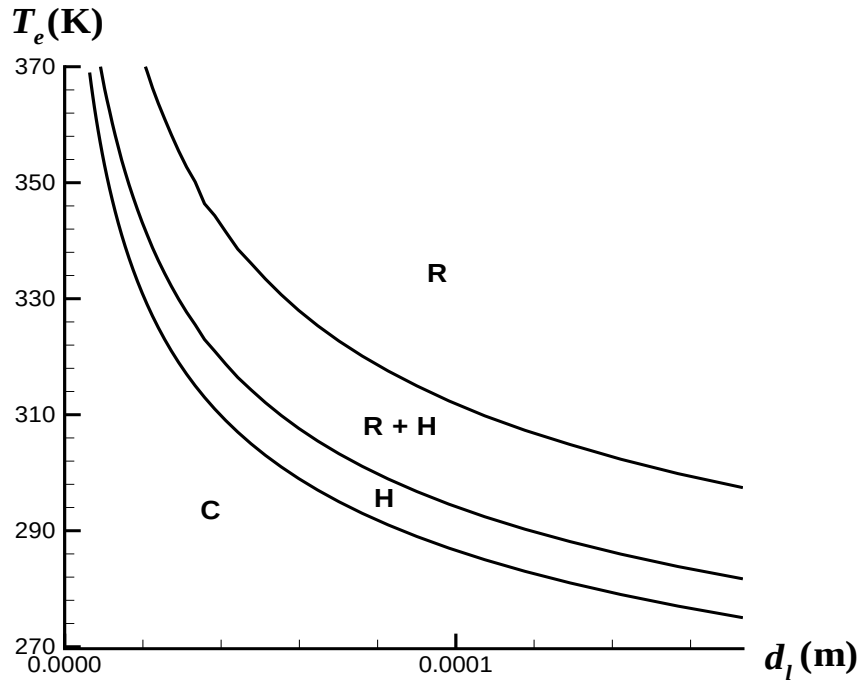

Figure 14: weakly nonlinear stability diagram for water ($\beta = 0.01$, $Y_{v,t} = 0$, $P_t = 1$ atm, $d_g = 0.0001$ m).

general tendency we note that squares are stable only below a critical value of d_l and rolls above this same value. As this critical depth is usually very small, we conclude that in the cases studied here and after the primary bifurcation to a hexagonal pattern, rolls are more easily observed than squares. Eventually note that in figures (13), (14) and (16) the Biot number not only changes along the neutral stability curves (as can be seen in table (2)), but also with the distance to threshold. We can see in figure (9), that for a given value of d_l, the Biot number increases with T_e. Table (2) shows that the Biot number is largely increased by the evaporation process, compared to the purely conductive case. Squares appear for values of the Biot number above approximately 1, which is in agreement with the results in [21].

Eventually note that these results, as the linear ones, are independent of β for values of $\beta \geq 0.01$ and change very little for lower values of β.

7 Summary

We have presented in this paper a linear and weakly nonlinear stability analysis of an evaporating liquid layer surmounted by an inert-gas vapor mixture. After reduction of the full two layer problem to a one-sided model, we performed a nonlinear stability analysis leading to a finite set of amplitude equations. A

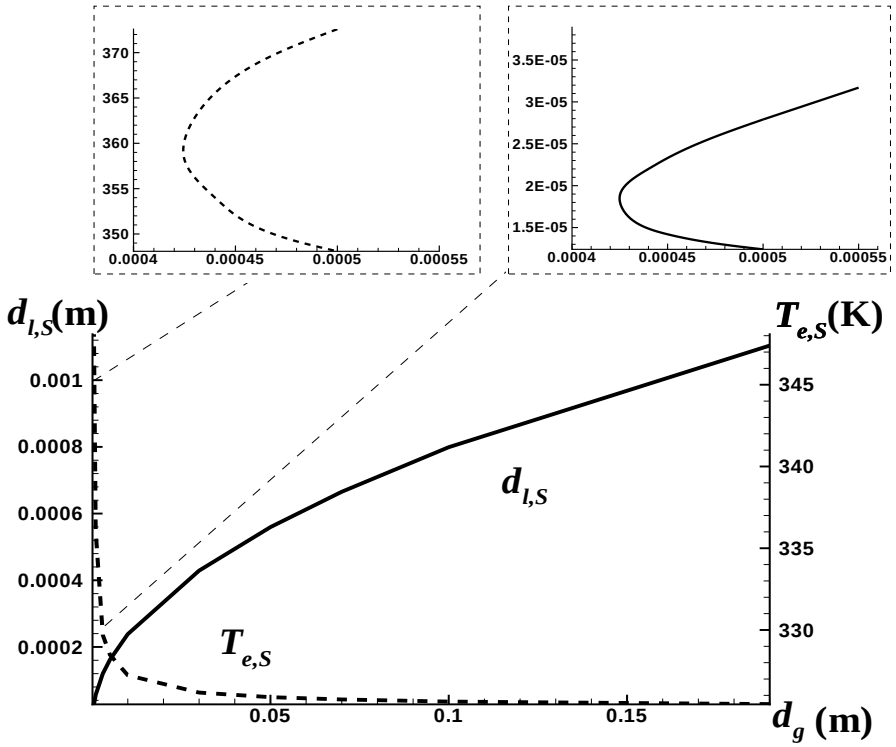

Figure 15: $d_{l,S}$ (full line, left axis) and $T_{e,S}$ (dashed line, right axis) as function of d_g ($\beta = 0.01$, $Y_{v,t} = 0$, $P_t = 1$ atm).

stability analysis of these amplitude equations permitted to draw a stability diagram of the roll, square and hexagonal pattern appearing above the linear stability threshold as a function of the liquid layer depth and the temperature. Both a water-air system and an ethanol-air system were considered. We found that squares are stable only below a critical value of the liquid depth and rolls above this same value. This critical depth is higher for an ethanol-air system than for a water-air system. Furthermore, we found that hexagons are the first pattern appearing past the linear stability threshold.

Note that the validity of our amplitude method is strictly speaking limited to the close neighborhood of the linear stability analysis, but it has been shown [24] that it can be extended to rather large values of ε.

Acknowledgments

The authors want to thank Professor G. Lebon and T. Desaive (Liège University) as well as P. Colinet (Bruxelles University) for fruitful discussions. This research has bee supported by the ESA MAP under contract No. AO-99-110 (CIMEX) and by the ESA PRODEX under contract No. 90160. M.D. acknowledges financial support from the F.R.I.A. (Fonds pour la Formation à la Recherche dans l'Industrie et dans l'Agriculture, Belgium).

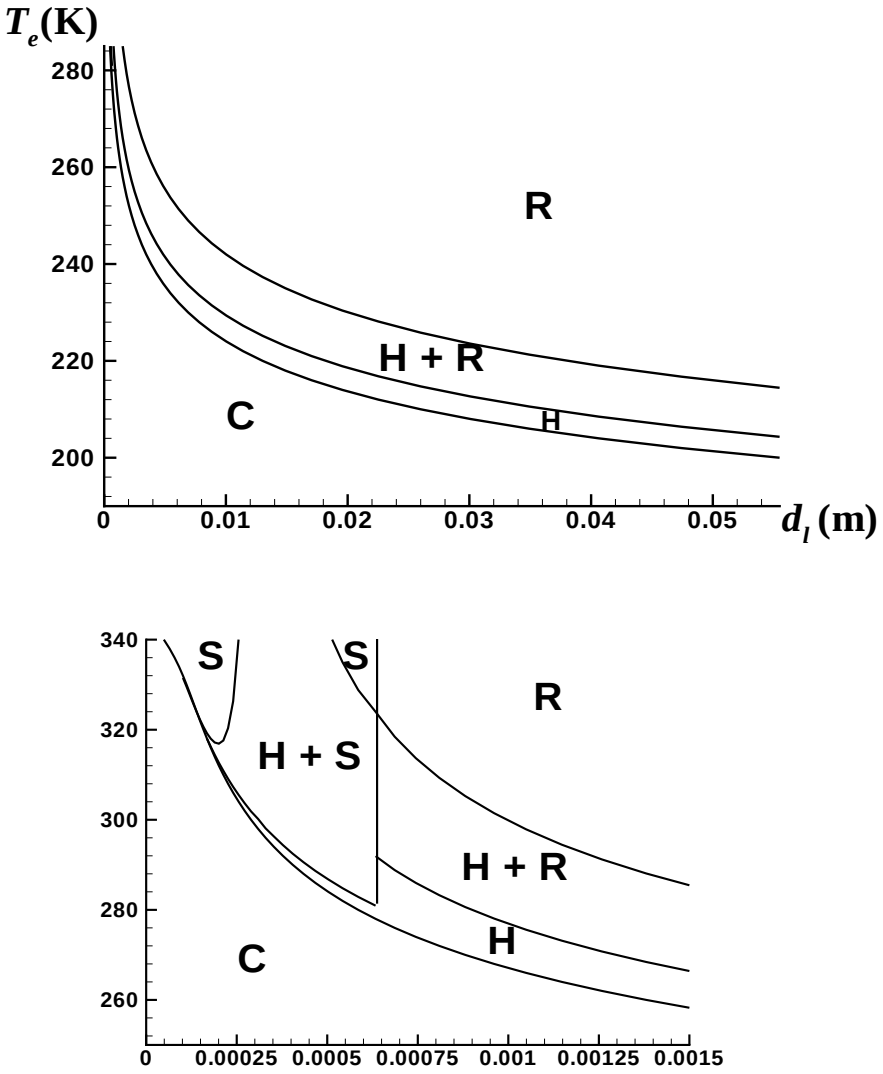

Figure 16: weakly nonlinear stability diagram for ethanol ($\beta = 0.01$, $Y_{v,t} = 0$, $P_t = 1$ atm, $d_g = 0.01$ m). The bottom figure is a zoom of the top one for low values of d_l and high values of T_e.

Table 2: $d_{l,c}$, $T_{e,c}$, Bi=$\mathrm{Bi}_{ev}+\lambda k_c coth(d_g^* k_c)$ and $\lambda k_c coth(d_g^* k_c)$ along the neutral stability curves of figures 13, 14 and 16

$d_{l,c}$(m)	$T_{e,c}$(K)	Bi	$\lambda k_c coth(d_g^* k_c)$
figure 13			
0.0001	355.6	2.648	0.0957
0.0002	329.6	1.065	0.0873
0.0005	301.3	0.375	0.0852
0.0010	284.5	0.208	0.0855
0.0015	276.0	0.161	0.0860
figure 14			
0.00001	353.7	0.574	0.0953
0.00005	303.7	0.283	0.0866
0.0001	286.6	0.196	0.0893
0.00020	272.3	0.180	0.1138
figure 16			
0.0001	332.3	9.023	0.4135
0.0002	312.1	3.095	0.3307
0.01	224.1	0.241	0.2294
0.03	208.0	0.350	0.3460
0.05	201.3	0.512	0.5091

References

[1] H. Bénard, Ann. Chem. Phys. 23 (1901) 62.

[2] D.A. Nield, J.Fluid Mech. 19 (1964) 341.

[3] J.R.A. Pearson, J.Fluid Mech. 4 (1958) 489.

[4] E.L. Koschmieder, Bénard Cells and Taylor Vortices, Cambridge University Press, Cambridge (1993).

[5] C. Normand, Y. Pomeau, M. Velarde, Rev.mod.Phys. 49 (1977) 581.

[6] P. Colinet, J.C. Legros, M.G. Velarde, Non Linear Dynamics of Surface Tension Driven Instabilities, Wiley-VCH, Berlin, 2001.

[7] J.C. Berg, M. Boudart, A. Acrivos, J. Fluid Mech. 24 (1966) 721.

[8] P. Colinet, L. Joannes, C.S. Iorio, B. Haut, M. Bestehorn, G. Lebon, J.C. Legros, Adv.Space Res. 32 (2003) 119.

[9] H. Mancini, D. Maza, Europhysics Letters 66 (6) (2004) 812-818.

[10] H.J. Palmer, J.Fluid Mech. 75 (1975) 487.

[11] F.J. Higuera, Phys. Fluids 30 (1987) 679.

[12] J.P. Burelbach, S.G. Bankoff, S.H. Davis, J.Fluid Mech. 195 (1988)463.

[13] B. Haut, P. Colinet, Submitted to J. Colloid Interface Sci.(2003).

[14] J. Margerit, G. Lebon, P. Colinet, C.S. Iorio, J.C. Legros, Phys. Rev. E 68 (2003) 041601.

[15] C. Moussy, G. Lebon, J. Margerit, Euro Phys. J. B. 40 (2004) 327-335.

[16] Vai-meng Ha, Chun-Liang Lai, Journal of the Chinese Institute of Engineers 21 (1998) 547.

[17] D. Merkt, M. Bestehorn, Physica D 185 (2003) 196.

[18] B. Haut, Master Thesis, Université Libre de Bruxelles, 2000.

[19] P.M. Parmentier, V.C. Regnier, G. Lebon, J.C. Legros, Phys. Rev. E 54 (1996) 411.

[20] M. Dondlinger, P. Colinet, P.C.Dauby, Phys. Rev. E 68 (2003) 066310.

[21] V. Regnier, P.C. Dauby, P. Parmentier, G. Lebon, Phys. Rev. E 55 (1997) 6860.

[22] R.C. Reid, J.M. Prausnitz, B.E. Poling, The properties of gases and liquids, McGraw-Hill Book Company, New York, 1987.

[23] Van P. Carey, Liquid-vapor phase change phenomena: An introduction to the Thermophysics of Vaporization and Condensation in Heat Transfer Equipment, Hemisphere Publishing Corporation, Washington, 1992.

[24] P.C. Dauby, Th. Desaive, J. Bragard, P. Cerisier, Phys. Rev. E 64 (2001) 066301.